Three-level algorithm to control COVID-19 spreading

Giovanni M. Dieguez
Universidade de São Paulo

Cristiane M. Batistela
Universidade de São Paulo

José Roberto C. Piqueira (✉ piqueira@lac.usp.br)
Universidade de São Paulo

Three-level algorithm to control COVID-19 spreading

Giovanni M. Dieguez, Cristiane M. Batistela & José Roberto C. Piqueira (corresponding author)

Abstract As the main ways of the coronavirus (COVID-19) spreading are air and physical contact, actions to mitigate and suppress its spreading must be developed in order to change population behavior, providing efficient control strategies. Here, these actions are described as a simple heuristic framework to establish public policies. The possible effects of these actions are modeled as a stratified control algorithm applied to an extension of the Susceptible-Infected-Removed (SIR) compartmental model. The model dynamics is analyzed and validated with simulations considering parameters obtained from epidemiological data from Brazil and Uruguay. Model simulations allow the proposition of a three-level control strategy that, as the numerical experiments show, presents promising results for the development of strategies to reduce the spread of COVID-19.

Keywords :
COVID-19; Equilibrium; SIRD; Social distancing; Stability.

1 Introduction

In the beginning of 2020, the epidemic of a new disease changed the history of humanity, being responsible for a global health and economic crisis. COVID-19 is a new coronavirus progeny, namely SARS-CoV-2 and was firstly reported in Wuhan, China, on December 31, 2019 [1,2]. A few months later, a report published by the World Health Organization qualified the disease as a pandemic due to its worldwide prevalence [3].

Giovanni M. Dieguez, Cristiane M. Batistela & José Roberto C. Piqueira (corresponding author)
Escola Politécnica da Universidade de São Paulo
Tel.: +55-11-30914488
E-mail: piqueira@usp.br *Av. Prof. Luciano Gualberto, tv. 3-158*
São Paulo-SP - Brazil

Transmission of SARS-CoV-2 occurs predominantly through physical transportation of contaminated droplets of secretions from an infected individual to an uninfected person, although the role of aerosol transmission and contaminated surface contact is currently unknown [4]. It is a disease with lower lethality when compared to its high transmission capacity, with the spreading aggravated by the average incubation time and due to both symptomatic and asymptomatic people being able to transmit the disease [5].

The disease has several forms of manifestation and most patients have rapid resolution, many of whom are asymptomatic. The initial symptoms are fever, cough and breathing difficulties. However, some patients with comorbidities may develop complications [6], requiring hospitalization, intensive treatment and mechanical respiratory ventilators, provoking a severe crisis in the health care system caused by the excessive number of hospitalizations.

To avoid overcrowded hospitals, different interventions aimed to slow the rapid evolution of the pandemic have been adopted by many countries. Strategies such as isolation of infected patients, mask wearing, regular hand hygiene, social distance, quarantine and total blocking of areas [7,?,?,?] were adopted all over the world.

Mathematical models are used to simulate the transmission of coronavirus and are helpful to understand the dynamical behavior of an infection, providing tools to estimate the duration and peaks of infection outbreaks and to design efficient control strategies [11,12,13]. Epidemiological mathematical models to be used here are present in health literature [14,15] related to several diseases, being helpful to define public actions to reduce COVID [16,17,18,19,20,21,22].

Development of macroscopic compartmental models for disease spreading has been research field since the Kermack and McKendrick proposition [23,24,25], dividing population into groups such as in Susceptible - Infected - Removed (SIR) or in Susceptible - Exposed - Infected - Removed (SEIR) models. Several modifications of the SIR model [26,27,28] have been proposed for epidemic modeling [29,30,31,32], being useful to public health policy makers [33].

Due to the urgency of COVID-19, researchers around the world accepted the challenge of outlining mathematical models for the new epidemic. Several mathematical models have already been formulated for the population dynamics of COVID-19 in several countries [10,34,35,36,37,38,39,40] and pioneer methods are structured upon Machine Learning and statistical models such as decision trees and linear regression [41] or even more powerful ones like artificial neural networks [42,?], showing promising results. Machine learning has also been used as an assistance to early detection [44] and prediction of severity [45] of COVID-19.
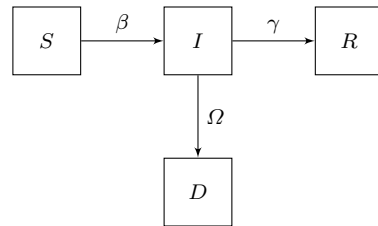
However, this paper considers a more classical and established approach, using the adjustment of social contact rate characterized by the control of the β parameter to mitigate COVID-19 spread. For this, a three-level controller is implemented and its relationship to social distance is validated. An extension of the compartmental SIR model is considered, the Susceptible - Infected -

Removed - Dead (SIRD) and the method is based on control theory, helping to define public policies to decrease the COVID-19 propagation [46].

Remaining paper is ordered as follows: in section 2, the equations and hypothesis of the model are presented. In section 3, the analysis of model dynamics is exhibited, the equilibrium points are determined, basic reproduction rate R_0 for the SIRD model is defined and analyzed with two simulations. Then, in section 4 the model is studied for the sake of establishing a baseline for the controller, with parameters derived using epidemic data from Brazil and Uruguay. Finally, section 5 outlines the controller and its effectiveness is investigated for a hypothetical scenario and the conclusions are shown at the end, in section 6. All simulations are performed with MATLAB Simulink.

2 Model formulation

The proposed model is a modification of the original SIR compartmental model [47], including a dead population compartment, here called Susceptible - Infected - Removed - Dead (SIRD) model, shown in figure (1). The model does not account for natural births and deaths as the Dead compartment being related only to deaths due to complications caused by the coronavirus infection.

Fig. 1 SIRD model.

Model parameters are described in table (I). β is the average number of contacts that result in contamination, per unit of time; γ is the recovery rate, i.e. the rate at which individuals leave the infected compartment after being recovered. Consequently, γ^{-1} represents the recovering time [48]. Additionally, Ω is the fraction of the infected population that dies, per unit of time (mortality rate).

Parameter	Parameter description
β	Average contact rate.
γ^{-1}	Mean infectious period.
Ω	Mortality rate.

Table I Model parameters.

As it can be observed, the model presents some simplifications:

– a recovered individual is supposed to acquire immunity and does not return to the susceptible compartment becoming "Removed" ("R" from SIRD);
– parameters β, γ and Ω are considered to be constants, despite depending on individual behavior, health care availability and age.

Under the described conditions, the model dynamics can be written as:

$$\begin{cases} \dot{S} & = -\dfrac{\beta SI}{N}, \\ \dot{I} & = \dfrac{\beta SI}{N} - (\gamma + \Omega)I, \\ \dot{R} & = \gamma I, \\ \dot{D} & = \Omega I. \end{cases} \tag{2.1}$$

with $N = S(t) + I(t) + R(t) + D(t)$ and $\dot{S}(t) + \dot{I}(t) + \dot{R}(t) + \dot{D}(t) = 0$.

As natural births and deaths are not taken into account, the total number of individuals in the populations is considered to be constant, and the dynamics of the dead compartment can be written as a function of the other compartments:

$$\begin{cases} D = N - S - I - R, \\ \dot{D} = -(\dot{S} + \dot{I} + \dot{R}). \end{cases} \tag{2.2}$$

Besides, the recovered compartment is dependent on the susceptible and infected populations:

$$\dot{R} = -\frac{\gamma}{\gamma + \Omega}(\dot{S} + \dot{I}). \tag{2.3}$$

Therefore, the system dynamics can be rewritten without the removed and the dead variables, without any loss of generality:

$$\begin{cases} \dot{S} & = -\dfrac{\beta SI}{N}, \\ \dot{I} & = \dfrac{\beta SI}{N} - (\gamma + \Omega)I. \end{cases} \tag{2.4}$$

3 System dynamics analysis

3.1 Equilibrium conditions

For the proposed SIRD model, equilibrium points can be obtained by applying the conditions $\dot{S} = 0$ and $\dot{I} = 0$. Then, it can be concluded that every point of the form $(S^*, 0)$ is an equilibrium point.

Equilibria at $I = 0$ are called disease-free, as opposed to equilibria at $I \neq 0$, which are called endemic [49]. The SIRD model presents the former but not the latter.

3.2 Equilibrium points classification

In order to analyze the local stability of these points, the Hartman-Grobman theorem is applied [50], and the general Jacobian (J) constructed as:

$$J(S,I) = \begin{bmatrix} \dfrac{\partial f_1}{\partial S} & \dfrac{\partial f_1}{\partial I} \\ \dfrac{\partial f_2}{\partial S} & \dfrac{\partial f_2}{\partial I} \end{bmatrix} = \begin{bmatrix} -\dfrac{\beta I}{N} & -\dfrac{\beta S}{N} \\ \dfrac{\beta I}{N} & \dfrac{\beta S}{N} - (\gamma + \Omega) \end{bmatrix}. \tag{3.5}$$

For $(S,I) = (S^*, 0)$ the Jacobian is reduced to:

$$J(S^*, 0) = \begin{bmatrix} 0 & -\dfrac{\beta S^*}{N} \\ 0 & \dfrac{\beta S^*}{N} - (\gamma + \Omega) \end{bmatrix}. \tag{3.6}$$

Hence, the eigenvalue set for the equilibrium points can be found by:

$$\lambda(\lambda - \frac{\beta S^*}{N} + \gamma + \Omega) = 0 \tag{3.7}$$

Which gives:

$$(0, \frac{\beta S^*}{N} - (\gamma + \Omega)) \tag{3.8}$$

as the eigenvalue set. Considering that one of the eigenvalues is equal to zero, it is worth noticing that the eigenvalue set obtained from the equilibrium points allows a local stability analysis, with three possibilities:

– If $\dfrac{\beta S^*}{N} - (\gamma + \Omega) > 0 \Rightarrow$ these fixed points are unstable [50], so there will be growth of cases for a small perturbation.
– If $\dfrac{\beta S^*}{N} - (\gamma + \Omega) < 0 \Rightarrow$ the Center-Manifold theorem must be applied in order to classify the stability condition.

Consequently, to proceed with the equilibrium stability analysis, all points satisfying $\dfrac{\beta S^*}{N} - (\gamma + \Omega) < 0$ and $S^* \geqslant 0$ are studied applying the Center-Manifold theorem.

Considering $S^* > 0$, a new parameter $\tau > 0$ is introduced in order to translate the system so that the point (S* = τ,0) is the origin (0,0) of the new system. This is done because the Center Manifold Theorem only refers to neighborhoods of the origin of the corresponding analyzed system. Consequently, the rewritten system, with $Z = S - S^*$ is given by:

$$\begin{cases} \dot{Z} &= -\dfrac{\beta(Z+\tau)I}{N}, \\[4mm] \dot{I} &= \dfrac{\beta(Z+\tau)I}{N} - (\gamma + \Omega)I. \end{cases} \tag{3.9}$$

Consequently, studying the system (2.4) around $(\tau,0)$ is the same as studying the new system (3.9) around $(0,0)$. Nevertheless, the rewritten system doesn't possess the same physical interpretation as the SIRD model. In addition, substitute parameters are introduced

$$\begin{cases} \phi &= \dfrac{\beta}{N}, \\[3mm] \alpha &= \gamma + \Omega, \end{cases} \tag{3.10}$$

in order to remove non-essential parameters regarding the interpretation of the stability condition. Then:

$$\begin{cases} \dot{Z} &= -\phi(Z+\tau)I, \\[3mm] \dot{I} &= \phi(Z+\tau)I - \alpha I. \end{cases} \tag{3.11}$$

Additionally, it is necessary to transform (3.11) into the form (A.18), as shown in Appendix A, by changing the basis into a basis of eigenvectors. Consequently:

$$\begin{cases} \dot{u} = -\left(\dfrac{\phi^3\tau^2}{(\alpha - \phi\tau)^2} - \dfrac{\phi^2\tau}{\alpha - \phi\tau}\right)v^2 - \left(\phi + \dfrac{\phi^2\tau}{\alpha - \phi\tau}\right)uv, \\[4mm] \dot{v} = (\phi\tau - \alpha)v + \phi uv + \dfrac{\phi^2\tau}{\alpha - \phi\tau}v^2. \end{cases} \tag{3.12}$$

Therefore,

$$\begin{cases} A = [0], \\ B = [\phi\tau - \alpha], \\ f(u,v) = -\left(\dfrac{\phi^3\tau^2}{(\alpha - \phi\tau)^2} - \dfrac{\phi^2\tau}{\alpha - \phi\tau}\right)v^2 - \left(\phi + \dfrac{\phi^2\tau}{\alpha - \phi\tau}\right)uv, \\ g(u,v) = \phi uv + \dfrac{\phi^2\tau}{\alpha - \phi\tau}v^2. \end{cases} \tag{3.13}$$

To find h(u), as Appendix A shows, it is necessary to consider that the coordinates of any point in the center manifold must satisfy the conditions

$$\begin{cases} y = h(x), \\ |x| < \delta, \\ h(0) = 0, \\ Dh(0) = \dot{h}(0) = 0, \end{cases} \tag{3.14}$$

from (A.19), which substituting on (A.18) gives

$$\begin{cases} \dot{h}(u)[Au + f(u, h(u))] = Bh(u) + g(u, h(u)) \quad \Longleftrightarrow \\ \dot{h}(u)[Au + f(u, h(u))] - Bh(u) - g(u, h(u)) = 0. \end{cases} \tag{3.15}$$

Now, after substituting (3.13) (with v = h(u)) into (3.15), it can be seen that h(u) = 0 is a solution of the partial differential equation (3.15). Then, the vector field restricted to the center manifold is given by

$$\dot{u} = 0. \tag{3.16}$$

Therefore, u = 0 is stable in (3.16). Thus, Theorem 2 from Appendix A guarantees that $(Z, I) = (0, 0)$ is stable for any parameter $0 \le \tau < \dfrac{N(\gamma + \Omega)}{\beta})$ and, consequently, $(S^*, 0)$ is stable for the same set.

To complete the stability analysis, the case with $S^* = \dfrac{N(\gamma + \Omega)}{\beta}$ is considered, i.e., the Center-Manifold theorem [50] is applied for:
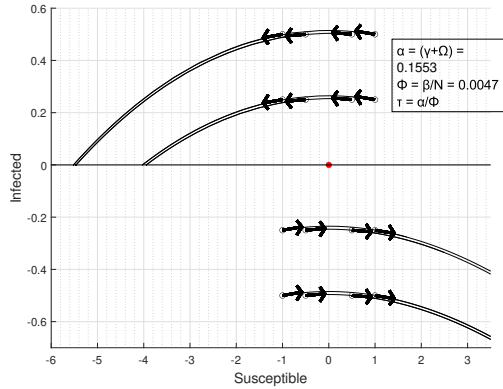
$$-\frac{\beta S*}{N} - (\gamma + \Omega) = 0.$$

The point $(S^* = \dfrac{N(\gamma + \Omega)}{\beta}, 0)$ is the origin of the system (3.11) with parameter $\tau = \dfrac{\alpha}{\phi}$. In order to assess stability, a simulation is presented in figure 2.

As it can be seen, neighborhoods close to the origin with initial values $I^* < 0$ are unstable, as the trajectories point towards negative infinite. However the system is only defined for $I^* > 0$, considering that there no negative infected. Although Z can be negative as the original system was translated and even a small disturbance would never produces a state with $I^* < 0$. Consequently, it is a degenerated equilibrium [51].

3.3 Basic reproduction rate

The basic reproduction rate R_0 is defined as the average number of secondary infections produced when one infected individual is introduced into a host population, where almost everyone is susceptible $(S \approx N)$ [13]. For example, if the R_0 for COVID-19 in a population is 5, then each new case is expected to produce 5 secondary infections, assuming everyone around is susceptible.

Fig. 2 Simulation around the origin for $\tau = \dfrac{\alpha}{\phi}$.

Mathematically, R_0 is a threshold for stability of a disease-free equilibrium and is related to the peak and final size of an epidemic [49].

Considering the equation

$$\dot{I} = \frac{\beta SI}{N} - (\gamma + \Omega)I,$$

from (2.4) it can observed that, when $S \approx N$, the signal of $\dot{I}$ is defined by $\beta - (\gamma + \Omega)$. Therefore, for the SIRD model, R_0 can be defined as

$$R_0 = \frac{\beta}{\gamma + \Omega}, \tag{3.17}$$

such that, when $R_0 > 1$ the equilibrium is locally unstable ($\dot{I} > 0$), but stable if $R_0 < 1$, implying $\dot{I} < 0$.
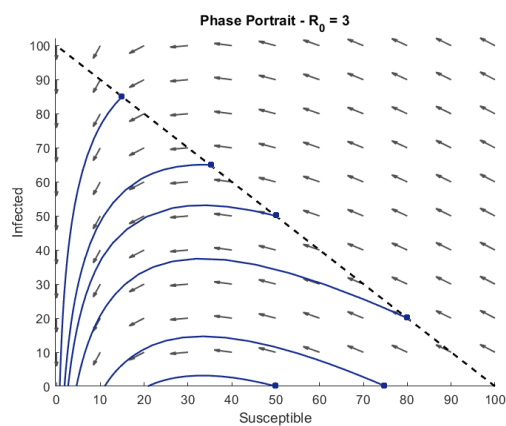
3.4 Phase portrait for different values of R_0

Figures (3) and (4) show the phase portrait of the system for different values of R_0, specifically chosen to portrait the only two possible outcomes.
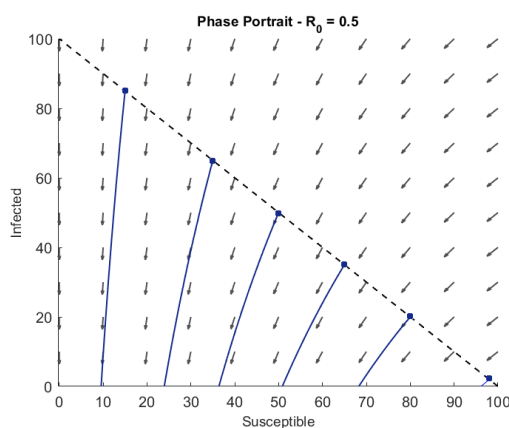
In (3), it is shown that, for $R_0 > 1$, the number of infected initially grows, but, as $\dot{S} < 0$, at some point $\dfrac{S^*}{N}$ eventually becomes $< \dfrac{1}{R_0}$, which implies $\dot{I} < 0$, and the trajectory always ends up in the horizontal axis (I = 0). This result is known as the herd immunity value.

The interception point depends on the initial conditions, therefore, there can be more or less individuals that will never become infected in the course of the epidemic (final number of susceptible at disease-free equilibrium).

In Figure (4), with $R_0 < 1$, the system points toward the horizontal axis much faster, with the number of infected decreasing steeply all time. This was to be expected as $\dot{I} < 0$ for $R_0 < 1$.
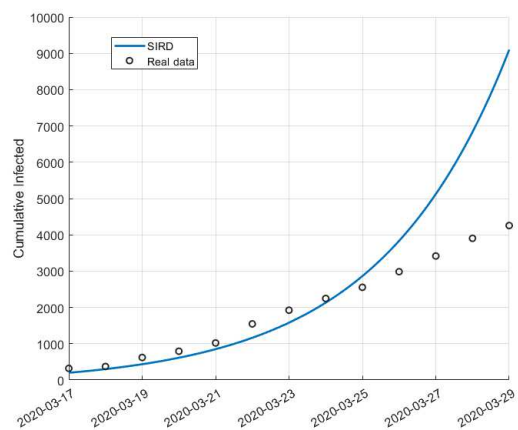
Fig. 3 Phase portrait for $R_0 = 3 \ (> 1)$.
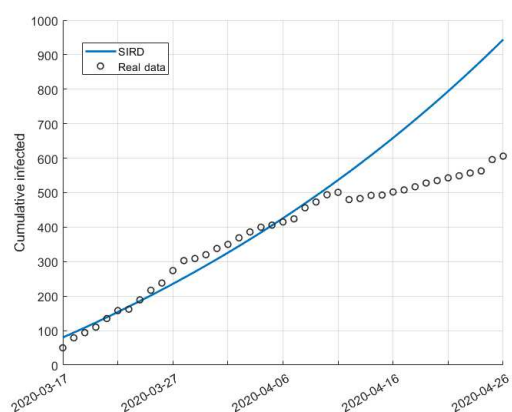

Fig. 4 Phase portrait for $R_0 = 0.5 < 1$.

4 Case studies and numerical simulations

In this section, two case studies are presented, with parameters derived from Brazil and Uruguay. These two countries were chosen because of their different basic reproduction number, as a result of particular population dynamics concerning the contact rate β. For Brazil, R_0 is estimated to be close to 2.82 [48] and for Uruguay, R_0 close to 1.13 [52]. These values were obtained using early infections data, as shown in figures (5) and (6), and are believed to present a scenario where there is no response to the pandemic, both individually or systemically.

Fig. 5 SIRD model validation with real data from Brazil. $R_0 = 2.82$, $\gamma = 0.1508$, $\Omega = 0.0045$.

Figure (5) and figure (6) compares SIRD model with real data from Brazil and Uruguay in the early days of disease spread, with the data source being [53].
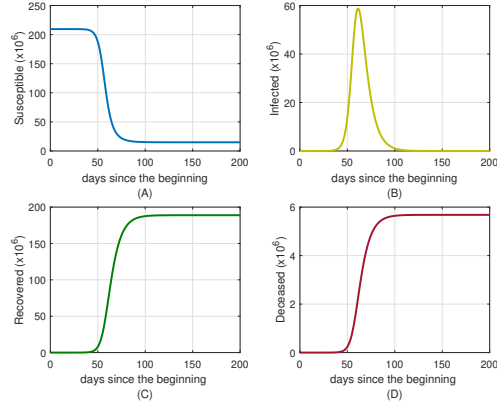

Fig. 6 SIRD model validation with real data from Uruguay. $R_0 = 1.13$, $\gamma = 0.1508$, $\Omega = 0.0045$. 2020-04-12 presents an anomaly in the dataset, with negative new cases.

Both graphs display a good fitting for initial data, with subsequent detachment between model and data, suggesting dynamical changes due to the implementation and effectiveness of isolation policies or individual confinement. In section 4.1 these set of parameters is used to simulate longer-term scenarios with no isolation that will serve as a reference for the evaluation of the control algorithm.
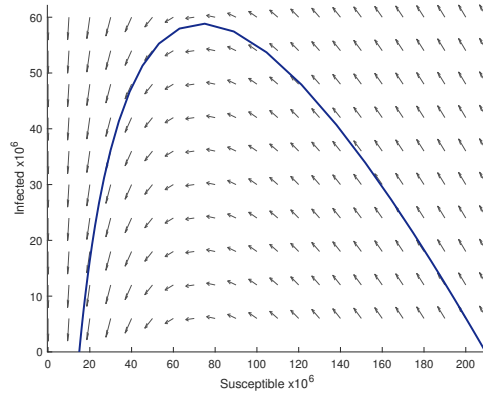
4.1 Simulation for Brazil

First, the model was simulated considering the parameters for Brazil, i.e., $N = 209.5$ million inhabitants, and $I_0 = 10$ individuals are considered, with the results shown in Figure 7.

Fig. 7 Brazilian case study. $R_0 = 2.82$, $\gamma = 0.1508$, $\Omega = 0.0045$.

The chosen parameters conduct the simulation to a full blown-out pandemic spread. The last case ended about 120 days after the disease had begun being disseminated as we can see in figure 5.B. Figure 5.D shows a high mortality figure at the pandemic end, i.e., about 2.71% of the total population before the pandemic.
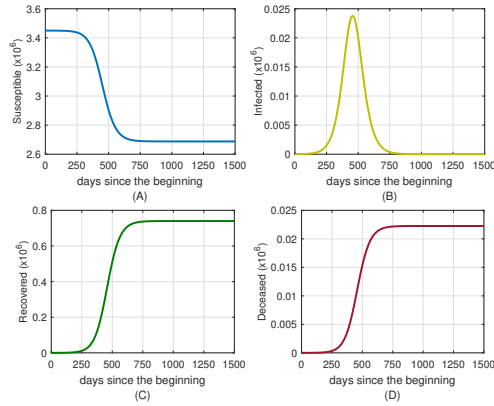

Fig. 8 Phase Portrait for Brazil, $R_0 = 2.82$ - axis in million.

Figure 8 shows clearly the large proportion of the population that became infected at some point. At the end, less than 10% never became infected.

4.2 Simulation for Uruguay

The model was also simulated with parameters from Uruguay, i.e., N = 3.45 million inhabitants, considering $I_0 = 10$ individuals, and results shown in Figure 9.

As R_0 for Uruguay is lower than Brazil's, there is significant differences concerning the dissemination of the virus. Figure 9 shows that the pandemic lasted much longer in Uruguay than in Brazil, however, Uruguay had fewer dead individuals at the end, only about 0.64% of the total population before the pandemic.
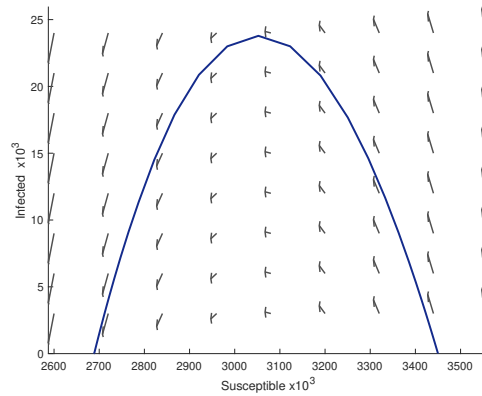

Fig. 9 Uruguay case study. $R_0 = 1.13$, $\gamma = 0.1508$, $\Omega = 0.0045$.

The low amount of individuals that ever got infected in Uruguay is highlighted in Figure 10, about 24% of the total population before the pandemic. Additionally, the lower number of infected suggests that having a lower R_0 due to lower β (contact rate) is a good indicator on what proportion the virus spread will achieve. This fact inspires the control algorithm used as reference of public policies employment, and is studied in the next section.

5 Spread control

Applications of Control Theory to Epidemiology range from Optimal Control, which can be used for social distancing [54], vaccine deployment policy [55], or even a mix of isolation and a vaccination program [56]; Model Predictive Control (MPC), which is also used to develop of social distancing [57,58] and

Fig. 10 Phase portrait Uruguay. $I_0 = 10$ individuals.

vaccination policies [59]. However, the approach to be followed here is simpler, and aims to build an algorithm explicitly programmed through a feedback of state variables, similar to other heuristics [60, ?] already studied.

Practical usage of the control algorithm proposed should consider the availability and uncertainty of current infections data, which are usually embedded with underreporting and significant delays when compared to reality, specially in countries which do not have a thorough testing program organized. It should review the simplifications assumed in the model formulation in section 2 as well, addressing the peculiarities of the disease being analyzed.

The present algorithm should address, in the future, any disease that follows the same pattern of transmission of the coronavirus, that is, infections resulted from the transportation of contaminated droplets of secretions from infected individuals to susceptible ones and that suggests isolation is effective. The main difference will be the difficulty imposed by a new virus concerning the imposition of lower values of R_t, parameter which will be described in next section. Viruses that are transmitted more easily impose a bigger challenge, as fewer contacts are needed to effectively pass the disease ahead.

5.1 Algorithm Implementation

Here, the implementation of a three-level stratified controller is studied, with the intention of mitigating the disease spread, aiming to maintain the demand of intensive care units (ICUs) lower than the available at all time, until a vaccine is available.

As it was shown, R_0 measures how the disease propagates when there are almost no infected individuals present ($S \approx N$). While R_0 provides valuable information on the viral dissemination dynamics when there is no developed immunity and information of the epidemic available, other factors begin to influence its dynamics during the spread course.

Therefore, the effective reproduction number R_t, which describes the average value of secondary infections as a time-dependent function, is a more appropriate parameter to be analyzed amidst an epidemic outbreak [62]. In a homogeneous population, it is simple to obtain R_t by multiplying R_0 and the susceptible proportion of the population at some instant t [63].

The idea to be developed is to regulate R_t in order to maintain the health care resources at an acceptable level. The underlying mechanism is the manipulation of the contact rate of individuals β by cycling the imposition and relaxation of social distancing measures [46] as well as awareness campaigns to stimulate adoption of individual protection procedures.

Therefore β is no longer considered fixed, but time-dependent $\beta(t)$. On the contrary, γ and Ω are still considered to be constant, as treatments such as the use of remdesivir or monoclonal antibodies, both approved by the American Federal Drug Administration (FDA), are prescribed only to severe cases whereupon the patient is already hospitalized and therefore, isolated [64,?] in the remdesivir case, while, for mono clonal antibodies, it is only approved for emergency use [66].

Levels of the controller are decided based on the current number of patients needing an ICU. This number is defined as 5% of the current number of infected individuals, assumed as the probability of someone who becomes infected to need intensive care [67].

Each level is composed of an interval from which R_t can assume randomly any value. The interval is constructed with limits equal to $\pm$ 10% of the measured mean value. This is done to mimic the difficulty of imposing and tracking a precise value for R_t for diseases with only a few epidemic studies.

The stratified controller model was chosen because it is easier to implement than other forms of modeling social distancing, generally based on continuous values for R_t, which are very hard to track and impose precisely. The algorithm is also adaptable structurally speaking as the R_t should necessarily guarantee the desired behavior according to the model. The biggest difficulties rest in creating the appropriate public policies to reach the desired R_t level.

Estimations of the economic impact of COVID-19 pandemic situate close to trillion dollars figures globally [73,74,75], with devastating shocks on various industries, and the imposition of social distancing policies should have been, theoretically, a big part of this loss. However, there is significant evidence that quarantine is effective against not implementing containment mechanisms [76], more effective when applied early [77], and that deterioration of economic conditions preceded the introduction of isolation policies [78] or that the culprit of COVID-19 recession is COVID-19 itself [79]. Therefore, practical usage of the three-level controller should lead to economic benefits, not to mention saving lives should be worth the cost nevertheless.

The three-level controller is described in Table II, with the calibration level (mitigation or suppression) related to the value of reproduction number associated. Mitigation and suppression measures differ in whether they aim to reduce the reproduction number, R_t, to less than 1 (suppression) or to merely slow spread by reducing R_t, but not to less than 1 (mitigation) [80]. Therefore,

Level A can be described as mitigation strategy and Level C as a suppression one, generally called a lock down, while Level B situates between both.

Level	$\mathbb{E}[R_t]$	Measures taken	Value source	When?
A	2	Self-imposed measures are stimulated in order to accelerate awareness spread. Prevention measures such as mask-wearing, hand-washing and self-imposed social distancing can be described as reductions in infectious output, susceptibility and contact rate, respectively [81].	As such measures stack up additively [81], a 10% efficacy on each one reduces the effective contact rate by 30%.	Intensive care unit demand is lower than 10% of the total amount available. $$\frac{5I}{100} < 5$$
B	1.1	Government implements social distancing measures such as reduced business hours and occupation or public spaces restrictions.	Similar to the R_t obtained for the state of Sao Paulo in March 2021, when such measures where adopted [82].	Intensive care unit demand is between 10-80% of the total amount available. $$5 < \frac{5I}{100} < 40$$
C	0.5	Mandatory home confinement except for vital sectors workers.	Very close to the R_t obtained by Spain during adoption of lock down [83].	Intensive care unit demand is higher than 80% of the total amount available. $$\frac{5I}{100} > 40$$

Table II Description of the three-level controller.

All the actions taken at a certain point will last for a regular chosen duration, during all the course of the pandemic. This is done in order to reduce social and economic uncertainty, as the population have time to comply.

6 Control strategy results

In this section, the three-level control strategy, described in the former section is simulated assuming an hypothetical scenario for an isolated city in Brazil with 10 infected initial cases, a population of 100,000 inhabitants and R_0 the same as the whole country (2.82). This number was maintained for the 15 initial days to replicate initial unawareness. Brazil is chosen due to its high baseline contact rate, represented by the high value of R_0, as opposed to Uruguay. Therefore, as the number of cases and individuals in need for ICUs grow faster than the system can adapt, it represents a need for the establishment of isolation policies.
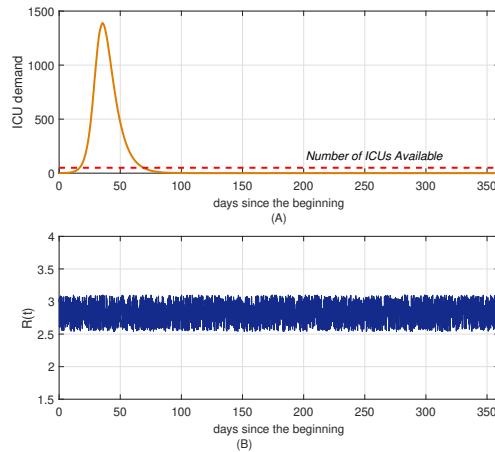
The number of ICUs available is considered to be 50, very close to the proportion of beds/individuals obtained for the state of Sao Paulo before the pandemic, in 2018 [68].

The total period analyzed is one year, because this is the period assumed for the development of a vaccine, with reference to the Pfizer vaccine, which started being developed January 2020 with the release of the SARS-CoV-2 genome [69], and initially applied in the UK at the beginning of December 2020 [70].

Three different strategies were considered: no attempt to control the disease spread; updating $R(t)$ every 30 days; and updating $R(t)$ every 21 days.

6.1 No attempt to control the spread of the disease

As expected, figure 11 shows the potential of COVID-19 to quickly overwhelm the health care system, with ICU demand surpassing the availability of beds less than two months after the beginning of the pandemic. The randomness added did not result in significant differences with respect to the baseline established in section 4.
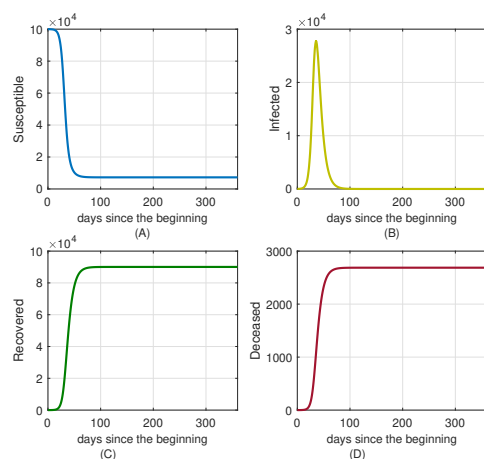

Fig. 11 No control applied.

The dynamics of free dissemination can be seen for all the compartments in the SIRD model used in figure 12.
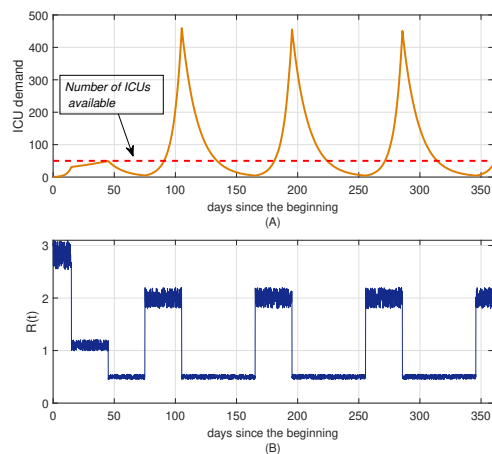
6.2 Updating $R(t)$ every 30 days

Figure 13 displays the algorithm's performance for a 30 day interval between updates regarding demand for ICU and shows the controlled reproductive

Fig. 12 State variables evolution when no control is applied.

number R_t for each cycle. It can be seen that, after periods of Level C (lock down), ICU demand went below 10% of the total number of intensive care beds available, which made the algorithm choose Level A for the following cycle.
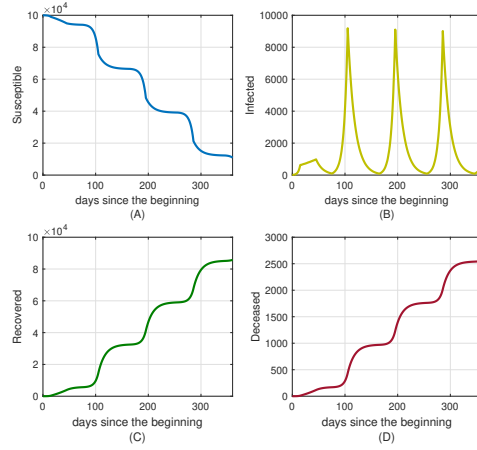
Every time that this happened, the control failed to prevent health care collapse, as 30 days proved to be enough time for Level A to allow a large increase of demand for ICU, due to the exponential growth nature of the spread.

Fig. 13 $R(t)$ control as measure of reducing COVID-19 spread.

The improvement over the baseline was very small, as can be seen in figure 12.D, with then number of deceased at the end of the period being very close to the number of deceased at the end in the baseline.

Therefore, in order to prevent the ICU demand from surpassing the supply of intensive care beds, the period between updates of the algorithm is reduced, and results shown in the next sub-section.

Fig. 14 System state variables.

6.3 Updating $R(t)$ every 21 days

For a 21 days interval between updates, the main goal of guaranteeing appropriate care for COVID-19 patients is attained. During the 360 days of simulation, there was no instant at which the demand for intensive care unit was bigger than the supply as shown by figure 15, and only three periods of Level C (lock down), allowing the individuals to have greater freedom without sacrificing effectiveness.

Figure 16 supports the effectiveness of the algorithm with 21 days cycle, showing much fewer deaths at the end of the simulation than in simulations I (baseline) and II (30 days cycle).
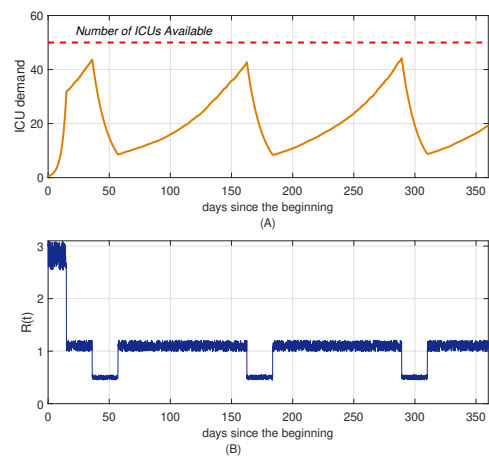
Fig. 15 $R(t)$ control as measure of reducing COVID-19 spread.
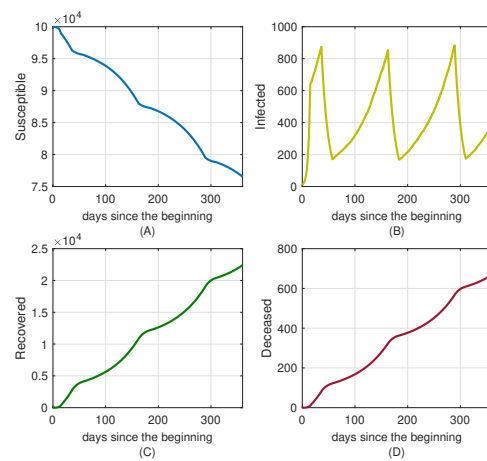

Fig. 16 System state variables.

7 Conclusions

Inspired by the different policies of social distances adopted by Brazil and Uruguay, showing remarkable differences concerning the results on controlling COVID-19 epidemic, a framework for modeling and applying public policies in the form of social distancing was proposed aiming the reduction of the disease spread.

A three-level controller was proposed and simulations indicate that a 21-day update strategy has shown good results, avoiding the health care system to collapse and presenting much fewer deaths at the end of the process.

To improve the model, it could be considered a varying R_t for each level and different number of levels. Uncertainties and delays could improve the observability of the number of infected cases.

Despite being an intuitively obvious conclusion, it was shown that not trying to mitigate the spread of the disease is not a wise option. The algorithm with 21 days between updates presents, for the example, almost 650 deaths at the end of the year, whereas doing nothing resulted in approximately 2700.

Therefore, it is possible to say that the framework outlined is a good and simple reference model to be followed when designing techniques to address the COVID-19 disease spread, and possibly other diseases that follow the same pattern of transmission as the corona virus.

Acknowledge

Conflict of interests

The authors declare that there is no conflict of interests regarding the publication of this article.

References

1. Velavan TP, Meyer CG. The COVID-19 epidemic. Trop Med Int Health 2020;25(3):278-80. https://doi.org/10.1111/tmi.13383
2. Wu Z, McGoogan JM. Characteristics of and important lessons from the coronavirus disease 2019 (COVID-19) outbreak in China: summary of a report of 72314 cases from the Chinese Center for Disease Control and Prevention. JAMA 2020;323(13):1239-42. https://doi.org/10.1001/jama.2020.2648
3. World Health Organization. WHO Director-General's opening remarks at the media briefing on COVID-19-11 March 2020.
4. Van Doremalen N, Bushmaker T, Morris DH, Holbrook MG, Gamble A, Williamson BN et al. Aerosol and surface stability of SARS-CoV-2 as compared with SARS-CoV-1. N Engl J Med 2020;382(16):1564-67. https://doi.org/10.1056/NEJMc2004973

5. Bai Y, Yao L, We T, Tian F, Jin DY, Chen L et al. Presumed asymptomatic carrier transmission of COVID-19. JAMA 2020;323(14):1406-07. 2020. https://doi.org/10.1001/jama.2020.2565

6. Sohrabi C, Alsafi Z, O'Neill N, Khan M, Kerwan A, Al-Jabir A, Iosifidis C et al. World Health Organization declares global emergency: A review of the 2019 novel coronavirus (COVID-19). Int J Surg 2020;76:71-6.https://doi.org/10.1016/j.ijsu.2020.02.034

7. Singh S, Parmar KS, Kumar J, Makkhan SJS. Development of new hybrid model of discrete wavelet decomposition and autoregressive integrated moving average (ARIMA) models in application to one month forecast the casualties cases of COVID-19. Chaos Solitons Fractals 2020;135:e109866. https://doi.org/10.1016/j.chaos.2020.109866

8. Prem K, Liu Y, Russell TW, Kucharski AJ, Eggo RM, Davies N. The effect of control strategies to reduce social mixing on outcomes of the COVID-19 epidemic in Wuhan, China: a modelling study. Lancet Public Health 2020;5(5):e261-e270. https://doi.org/10.1016/S2468-2667(20)30073-6

9. Colbourn T. COVID-19: extending or relaxing distancing control measures. Lancet Public Health 2020;5(5):e236-e237. https://doi.org/10.1016/S2468-2667(20)30072-4

10. Mishra BK, Keshri AK, Rao YS, Mishra BK, Mahato B, Ayesha S et al. COVID-19 created chaos across the globe: Three novel quarantine epidemic models. Chaos Solitons Fractals 2020;138:e109928. https://doi.org/10.1016/j.chaos.2020.109928

11. Anderson RM, May RM. Infectious diseases of humans: dynamics and control. Oxford University Press, 1992.

12. Brauer F, Castillo-Chavez C. Mathematical models in population biology and epidemiology, New York: Springer; 2012, Vol 2:p.508.

13. Hethcote HW. The mathematics of infectious diseases. SIAM Rev 2000;42(4):599-653. https://doi.org/10.1137/S0036144500371907

14. Dietz K. The first epidemic model: a historical note on PD En'ko. Aust J Stat 1998;30(1):56-65. https://doi.org/10.1111/j.1467-842X.1988.tb00464.x

15. Laarabi H, Abta A, Hattaf K. Optimal control of a delayed SIRS epidemic model with vaccination and treatment. Acta Biotheor 2015;63(2):87-97. https://doi.org/10.1007/s10441-015-9244-1

16. Aldila D, Gtz T, Soewono F. An optimal control problem arising from a dengue disease transmission model. Math Biosci 2013;242(1):9-16. https://doi.org/10.1016/j.mbs.2012.11.014

17. Ruan S, Xiao D, Beier JC. On the delayed Ross-Macdonald model for malaria transmission. Bull Math Biol 2008;70(4):1098-1114. https://doi.org/10.1007/s11538-007-9292-z

18. Nwankwo A, Okuonghae D. A mathematical model for the population dynamics of malaria with a temperature dependent control. Differ Equ Dyn Syst 2019;1-30. https://doi.org/10.1007/s12591-019-00466-y

19. Egonmwan AO, Okuonghae D. Mathematical analysis of a tuberculosis model with imperfect vaccine. Int J Biomath 2019;12(07):e1950073. https://doi.org/10.1142/S1793524519500736

20. Omame A, Okuonghae D, Umana AR, Inyama SC. Analysis of a co-infection model for HPV-TB. Appl Math Model 2020;77:881-901. https://doi.org/10.1016/j.apm.2019.08.012

21. Omame A, Okuonghae D, Inyama SC. A Mathematical Study of a Model for HPV with Two High-Risk Strains. In: Mathematical Modelling in Health, Social and Applied Sciences, Springer Singapore; 2020, p.107-149.

22. Hattaf K, Yousfi N. Optimal control of a delayed HIV infection model with immune response using an efficient numerical method. Int Sch Res Notices 2012;2012:e215124. https://doi.org/10.5402/2012/215124

23. Kermack WO, McKendrick AG. A contribution to the mathematical theory of epidemics. Proc R Soc Lond A 1927;115(772):700-721. https://doi.org/10.1098/rspa.1927.0118

24. Kermack WO, McKendrick AG. Contributions to the mathematical theory of epidemics. II. - The problem of endemicity. Proc R Soc Lond A 1932;138(834):55-83. https://doi.org/10.1098/rspa.1932.0171

25. Kermack WO, McKendrick AG. Contributions to the mathematical theory of epidemics. III. Further studies of the problem of endemicity. Proc R Soc Lond A 1933;141(843):94-122. https://doi.org/10.1098/rspa.1933.0106

26. Cant B, Coll C, Snchez E. Estimation of parameters in a structured SIR mode. Adv Differ Equ 2017;2017(1):e33. https://doi.org/10.1186/s13662-017-1078-5
27. Ng TW, Turinici G, Danchin A. A double epidemic model for the SARS propagation. BMC Infect Dis 2003;3(1):1-16. https://doi.org/10.1186/1471-2334-3-19
28. Danca MF, Kuznetsov N. Matlab code for Lyapunov exponents of fractional-order systems. Int J Bifurcat Chaos 2018;28(05):e1850067. https://doi.org/10.1142/S0218127418500670
29. Godio A, Pace F, Vergnano A. SEIR modeling of the Italian epidemic of SARS-CoV-2 using computational swarm intelligence. Int J Environ Res Public Health 2020;17(10):e3535, 2020. https://doi.org/10.3390/ijerph17103535
30. Lin Q, Zhao S, Gao D, Lou Y, Yang S, Musa SS et al. A conceptual model for the coronavirus disease 2019 (COVID-19) outbreak in Wuhan, China with individual reaction and governmental action. Int J Infect Dis 2020;93:211-216. https://doi.org/10.1016/j.ijid.2020.02.058
31. Piqueira JRC, Araujo VO. A modified epidemiological model for computer viruses. Appl Math Comput 2009;213(2):355-360. https://doi.org/10.1016/j.amc.2009.03.023
32. Piqueira JRC, Batistela CM. Considering quarantine in the SIRA malware propagation model. Math Probl Eng 2019;2019:e6467104. https://doi.org/10.1155/2019/6467104
33. Khajanchi S, Das DK, Kar TK. Dynamics of tuberculosis transmission with exogenous reinfections and endogenous reactivation. Physica A 2018;497:52-71. https://doi.org/10.1016/j.physa.2018.01.014
34. Mizumoto K, Chowell G. Transmission potential of the novel coronavirus (COVID-19) onboard the diamond Princess Cruises Ship. Infect Dis Model 2020;5:264-270. https://doi.org/10.1016/j.idm.2020.02.003
35. Atangana A. Modelling the spread of COVID-19 with new fractal-fractional operators: Can the lockdown save mankind before vaccination?. Chaos Solitons Fractals 2020;136:e109860. https://doi.org/10.1016/j.chaos.2020.109860
36. Hellewell J, Abbott S, Gimma A, Bosse NI, Jarvis CI, Russell TW et al. Feasibility of controlling COVID-19 outbreaks by isolation of cases and contacts. Lancet Glob Health 2020;8(4):e488-e496. https://doi.org/10.1016/S2214-109X(20)30074-7
37. Ivorra B, Ferrndez MR, Vela-Prez M, Ramos AM. Mathematical modeling of the spread of the coronavirus disease 2019 (COVID-19) taking into account the undetected infections. The case of China. Commun Nonlinear Sci Numer Simul 2020;88:e105303. https://doi.org/10.1016/j.cnsns.2020.105303
38. Higazy H. Novel fractional order SIDARTHE mathematical model of COVID-19 pandemic. Chaos Solitons Fractals 2020;138:e110007. https://doi.org/10.1016/j.chaos.2020.110007
39. Samui P, Mondal J, Khajanchi S. A mathematical model for COVID-19 transmission dynamics with a case study of India. Chaos Solitons Fractals 2020;140:e110173. https://doi.org/10.1016/j.chaos.2020.110173
40. Batistela CM, Correa DP, Bueno AM, Piqueira JRC. SIRSi compartmental model for COVID-19 pandemic with immunity loss. Chaos Solitons Fractals 2021;142:e110388. https://doi.org/10.1016/j.chaos.2020.110388
41. Malki Z, Atlam E, Ewis A, Dagnew G et al. The COVID-19 pandemic: prediction study based on machine learning models. Environ Sci Pollut Res 2021;28:4049640506.
42. Wieczorek M, Silka J, Polap D, Wozniak M et al. Real-time neural network based predictor for cov19 virus spread. PLOS One 2020;15(12):e0243189. https://doi.org/10.1371/journal.pone.0243189
43. Braga MB, Fernandes RS, Souza Jr GN, Rocha EC et al. Artificial neural networks for short-term forecasting of cases, deaths, and hospital beds occupancy in the COVID-19 pandemic at the Brazilian Amazon. PLoS ONE 2021;16(3):e0248161. https://doi.org/10.1371/journal.pone.0248161
44. Iwendi C, Khalid K et al. Classification of COVID-19 individuals using adaptive neuro-fuzzy inference system. Multimedia Syst 2021. https://doi.org/10.1007/s00530-021-00774-w
45. Iwendi C, Kashif BA et al. COVID-19 Patient Health Prediction Using Boosted Random Forest Algorithm. Frontiers in Public Health 2020;8:357. doi.org/10.3389/fpubh.2020.00357

46. Stewart G, van Heusden K, Dumont GA. How Control Theory Can Help Us Control COVID-19. IEEE Spectr [internet]. 2020 Jul [cited 2021 Apr 21]. Available from: https://spectrum.ieee.org/biomedical/diagnostics/how-control-theory-can-help-control-covid19 No subscription required.

47. Murray JD. Mathematical biology. 3rd ed. Springer New York; 2002.

48. Bastos SB, Cajueiro DO. Modeling and forecasting the early evolution of the COVID-19 pandemic in Brazil. Sci Rep 2020;10:e19457. https://doi.org/10.1038/s41598-020-76257-1

49. Brauer F, van den Driessche P, Wu J. Mathematical Epidemiology. 1st ed. Springer; 2008.

50. Guckenheimer J, Holmes P. Nonlinear Oscillations, Dynamical Systems and Bifurcation of Vector Fields. 1st ed. Springer New York; 1983.

51. Andronov AA, Vitt AA, Khaikin SE. Theory of Oscillators. 1st ed. Pergamon; 1966.

52. Dutra C. Estimate of the basic number of reproduction R0 of COVID-19 in South American countries. Interam J Med Health 2020;3:1-7. https://doi.org/10.31005/iajmh.v3i0.127

53. Our World in Data. Coronavirus (COVID-19) Cases. https://ourworldindata.org/covid-cases; 2021 [accessed 07 Sep 2021].

54. Kruse T, Strack P. Optimal Control of an Epidemic Through Social Distancing. Cowles Found Discussion Pap 2020;2229. http://dx.doi.org/10.2139/ssrn.3583186

55. Jaberi-Douraki M, Moghadas SM. Optimal control of vaccination dynamics during an influenza epidemic. Math Biosci Eng 2014;11(5):1045-1063. https://doi.org/10.3934/mbe.2014.11.1045

56. Hansen E, Day T. Optimal control of epidemics with limited resources. J Math Biol 2011;62:423451. https://doi.org/10.1007/s00285-010-0341-0

57. Morato MM, Bastos SB, Cajueiro DO, Normey-Rico JE. An optimal predictive control strategy for COVID-19 (SARS-CoV-2) social distancing policies in Brazil. Annual Reviews in Control 2020; 50:417-431. https://doi.org/10.1016/j.arcontrol.2020.07.001

58. Khler J, Schwenkel L, Koch A, Berberich J, Pauli P, Allgwer F. Robust and optimal predictive control of the COVID-19 outbreak. Annual Reviews in Control 2021; 51:525-539. https://doi.org/10.1016/j.arcontrol.2020.11.002

59. Khler J, Enyler2ioha C, Allgwer F. Dynamic Resource Allocation to Control Epidemic Outbreaks A Model Predictive Control Approach. Ann Amer Contr Conf 2018, 1546-1551. https://doi.org/10.23919/ACC.2018.8431769

60. Bin M, Cheung PYK, Crisostomi E, Ferraro P et al. Post-lockdown abatement of COVID-19 by fast periodic switching. PLOS Comput Biol 2021; 17(1):1008604. https://doi.org/10.1371/journal.pcbi.1008604

61. Meidan D, Schulmann N, Cohen R, Haber Simcha et al. Alternating quarantine for sustainable epidemic mitigation. arXiv:2004.01453.

62. Khailaie S, Mitra T, Bandyopadhyay A, Schips M, Mascheroni P, Vanella P et al. Development of the reproduction number from coronavirus SARS-CoV-2 case data in Germany and implications for political measures. BMC Med 2021;19:e32. https://doi.org/10.1186/s12916-020-01884-4

63. Garnett GP. Role of Herd Immunity in Determining the Effect of Vaccines against Sexually Transmitted Disease. J Infect Dis 2005;191:S97S106. https://doi.org/10.1086/425271

64. Centers for Disease Control and Prevention. Information for Clinicians on Investigational Therapeutics for Patients with COVID-19, https://www.cdc.gov/coronavirus/2019-ncov/hcp/therapeutic-options.html; 2020 [accessed 13 Mar 2021].

65. Johns Hopkins Medicine. Is the Coronavirus Treatable?, https://www.hopkinsmedicine.org/health/conditions-and-diseases/coronavirus/coronavirus-treatment-whats-in-development; 2020 [accessed 05 Apr 2021].

66. FDA. Coronavirus (COVID-19) Update: FDA Authorizes Monoclonal Antibodies for Treatment of COVID-19. https://www.fda.gov/news-events/press-announcements/coronavirus-covid-19-update-fda-authorizes-monoclonal-antibodies-treatment-co 2020 [accessed 07 Sep 2021].

67. Guan W, Ni Z, Yu Hu, Liang W, Ou C, He J et al. Clinical Characteristics of Coronavirus Disease 2019 in China. N Engl J Med 2020;382:1708-1720.https://doi.org/10.1056/NEJMoa2002032
68. Conselho Federal de Medicina. Medicina Intensiva no Brasil, https://portal.cfm.org.br/images/PDF/leitosdeuticapitais2018.pdf; 2018 [accessed 25 Mar 2021].
69. Ball P. The lightning-fast quest for COVID vaccines and what it means for other diseases. Nature 2021;589:16-18. https://doi.org/10.1038/d41586-020-03626-1
70. CNN. UK becomes first country to authorize Pfizer/BioNTech's COVID-19 vaccine, first shots roll out next week. https://edition.cnn.com/2020/12/02/uk/pfizer-coronavirus-vaccine-uk-intl-hnk/index.html; 2020 [acessed 17 Apr 2021].
71. Moler CB. Numerical Computing with MATLAB. 1st ed. SIAM Philadelphia; 2004.
72. Ogata K. Modern Control Engineering. 1st ed. Prectice-Hall; 1990.
73. UN. COVID-19 to slash global economic output by \$8.5 trillion over next two years. https://www.un.org/en/desa/covid-19-slash-global-economic-output-85-trillion-over-next-two-years; 2020 [accessed 09 Sep 2021].
74. UN. Global economy could lose over \$4 trillion due to COVID-19 impact on tourism. https://unctad.org/news/global-economy-could-lose-over-4-trillion-due-covid-19-impact-tourism; 2021 [accessed 9 Sep 2021].
75. Global Economic Effects of COVID-19 (CRS Report No. R46270). Retrieved from Congressional Research Service website: https://crsreports.congress.gov/; 2021 [accessed 8 Sep 2021].
76. Gupta AG, Moyer CA, Stern DT. The economic impact of quarantine: SARS in Toronto as a case study. J Infection 2005; 50(5):386-393.
77. Demirg-Kunt A, Lokshin M, Torre Ivn. The Sooner, the Better: The Early Economic Impact of Non-Pharmaceutical Interventions During the COVID-19 Pandemic. World Bank Policy Research Working Paper No 9257 2020.
78. Chen S, Igan DO, Pierri N, Presbitero AF et al. Tracking the Economic Impact of COVID-19 and Mitigation Policies in Europe and the United States. IMF 2020; 2020(125):25.
79. Aum S, Yoon Sang, Shin Yongseok. COVID-19 doesnt need lockdowns to destroy jobs: The effect of local outbreaks in Korea. Labour Econ 2021; 70:e101993.
80. Imperial College London. Report 9 - Impact of non-pharmaceutical interventions (NPIs) to reduce COVID-19 mortality and healthcare demand, https://www.imperial.ac.uk/media/imperial-college/%5Cmedicine/sph/ide/gida-fellowships/Imperial-College-COVID19-NPI-modelling-2020 [accessed 8 Apr 2021].
81. Teslya A, Pham TM, Godijk NG, Kretzschmar ME, Bootsma MCJ, Rozhnova G. Impact of self-imposed prevention measures and short-term government-imposed social distancing on mitigating and delaying a COVID-19 epidemic: A modelling study. PLoS Med 2020;17(7):e1003166. https://doi.org/10.1371/journal.pmed.1003499
82. G1. Governo de SP avana 6 regies para a fase amarela da quarentena, que permite funcionamento de restaurantes at 22h, https://g1.globo.com/sp/sao-paulo/noticia/2021/02/05/governo-de-sp-avanca-6-regioes-para-a-fase-amarela-que-permite-funcionamento-2021 [accessed 28 Mar 2021].
83. Hyafil A, Moria D. Analysis of the impact of lockdown on the reproduction number of the SARS-Cov-2 in Spain. Gac Sanit, 2020. https://doi.org/10.1016/j.gaceta.2020.05.003
84. Wiggins S. Introduction to Applied Nonlinear Dynamical Systems and Chaos. 1st ed. Springer New York; 1990.

Appendix A

From (Wiggins, 1990, p.193) [84].

Consider vector fields of the form

$$
\begin{cases}
\dot{x} = Ax + f(x, y), \\
\dot{y} = By + g(x, y), \quad (x, y) \in \mathbb{R}^c \times \mathbb{R}^s,
\end{cases}
\tag{A.18}
$$

satisfying

$$
\begin{aligned}
f(0, 0) &= 0, \quad Df(0, 0) = 0, \\
g(0, 0) &= 0, \quad Dg(0, 0) = 0,
\end{aligned}
$$

where A is a c×c matrix having eigenvalues with zero real parts, B is an s×s having eigenvalues with negative real part, and f and g are $\mathbf{C}^r$ functions (r≥2). Then:

Remark 1 *An invariant manifold will be called a center manifold for (A.18) if it can locally be represented as*

$$
W^c(0) = \{(x, y) \in \mathbb{R}^c \times \mathbb{R}^s | y = h(x), |x| < \delta, h(0) = 0, Dh(0) = 0\} \tag{A.19}
$$

for δ sufficiently small.

Theorem 1 *There exists a $\mathbf{C}^r$ center manifold for (A.18). The dynamics of (A.18) restricted to the center manifold is, for u sufficiently small, given by the following c-dimensional vector field*

$$
\dot{u} = Au + f(u, h(u)), \quad u \in \mathbb{R}^c. \tag{A.20}
$$

Theorem 2 *i) Suppose the zero solution of (A.20) is stable (asymptotically stable) (unstable); then the zero solution of (A.18) is also stable (asymptotically stable) (unstable). ii) Suppose the zero solution of (A.20) is stable. Then if $(x(t), y(t))$ is a solution of (A.18) with $(x(0), y(0))$ sufficiently small, there is a solution u(t) of (A.20) such that as $t \to \infty$*

$$
\begin{aligned}
x(t) &= u(t) + \mathcal{O}(e^{-\gamma t}), \\
y(t) &= h(u(t)) + \mathcal{O}(e^{-\gamma t}),
\end{aligned}
$$

where $\gamma > 0$ is a constant.